International Journal of Applied Earth Observation and Geoinformation 53 (2016) 16–26

Contents lists available at ScienceDirect

International Journal of Applied Earth Observation and Geoinformation

journal homepage: www.elsevier.com/locate/jag

Plant species discrimination using emissive thermal infrared imaging spectroscopy

Gilles Rock[a,*], Max Gerhards[a,b], Martin Schlerf[b], Christoph Hecker[c], Thomas Udelhoven[a,b]

[a] Environmental Remote Sensing & Geoinformatics Department, Faculty of Geography and Geosciences, University of Trier, Behringstrasse, D-54286 Trier, Germany
[b] Department of Environmental Research and Innovation, Luxembourg Institute of Science and Technology (LIST), 41 Rue du Brill, L-4422 Belvaux, Luxembourg
[c] Faculty of Geo-Information Science and Earth Observation (ITC), University of Twente, P.O. Box 217, 7500 AE Enschede, The Netherlands

ARTICLE INFO

Article history:
Received 6 June 2016
Received in revised form 4 August 2016
Accepted 5 August 2016
Available online 10 August 2016

Keywords:
Hyperspectral thermal infrared
Emissivity spectra
Temperature emissivity separation
Species discrimination

ABSTRACT

Discrimination of plant species in the optical reflective domain is somewhat limited by the similarity of their reflectance spectra. Spectral characteristics in the visible to shortwave infrared (VSWIR) consist of combination bands and overtones of primary absorption bands, situated in the Thermal Infrared (TIR) region and therefore resulting in broad spectral features. TIR spectroscopy is assumed to have a large potential for providing complementary information to VSWIR spectroscopy. So far, in the TIR, plants were often considered featureless. Recently and following advances in sensor technology, plant species were discriminated based on specific emissivity signatures by Ullah et al. (2012) using directional-hemispherical reflectance (DHR) measurements in the laboratory. Here we examine if an accurate discrimination of plant species is equally possible using emissive thermal infrared imaging spectroscopy, an explicit spatial technique that is faster and more flexible than non-imaging measurements.

Hyperspectral thermal infrared images were acquired in the 7.8–11.56 μm range at 40 nm spectral resolution (@10 μm) using a TIR imaging spectrometer (Telops HyperCam-LW) on seven plants each, of eight different species. The images were radiometrically calibrated and subjected to temperature and emissivity separation using a spectral smoothness approach. First, retrieved emissivity spectra were compared to laboratory reference spectra and then subjected to species discrimination using a random forest classifier. Second, classification results obtained with emissivity spectra were compared to those obtained with VSWIR reflectance spectra that had been acquired from the same leaf samples.

In general, the mean emissivity spectra measured by the TIR imaging spectrometer showed very good agreement with the reference spectra (average Nash-Sutcliffe-Efficiency Index = 0.64). In species discrimination, the resulting accuracies for emissivity spectra are highly dependent on the signal-to-noise ratio (SNR). At high SNR, the TIR data (Overall Accuracy (OAA) = 92.26%) outperformed the VSWIR data (OAA = 80.28%).

This study demonstrates that TIR imaging spectroscopy allows for fast and spatial measurements of spectral plant emissivity with accuracies comparable to laboratory measurement. This innovative technique offers a valuable addition to VSWIR spectroscopy as it provides complimentary information for plant species discrimination.

1. Introduction

Vegetation mapping and species discrimination are key requirements of studies focusing on ecosystem monitoring and development. The time consuming traditional methods of in-field mapping are optimized by remote sensing data collection, which facilitates the economic acquisition of repeated data products allowing for large area studies of vegetation cover (Langley et al., 2001). Remote sensing based vegetation mapping has been achieved in different ways including multi-spectral, hyperspectral, and multi-temporal classification (Langley et al., 2001; White et al., 2005).

* Corresponding author.
E-mail address: rock@uni-trier.de (G. Rock).

http://dx.doi.org/10.1016/j.jag.2016.08.005
0303-2434/

Table 1
The studied plant species with their common name, Latin name, sample size and short code.

Common name	Latin name	Sample size(nr plants x nr. leaves)	Short code
Vine Peach	*Prunus persica*	35 (7 × 5)	*Pp*
Sweetgum	*Liquidambar styraciflua*	35 (7 × 5)	*Ls*
Redosier dogwood	*Cornus sericea*	35 (7 × 5)	*Cs*
Maidenhair tree	*Ginkgo biloba*	35 (7 × 5)	*Gb*
Cherry laurel	*Prunus lauracerasus*	35 (7 × 5)	*Pl*
Rhododendron	*Rhododendron repens*	35 (7 × 5)	*Rr*
David viburnum	*Viburnum davidii*	35 (7 × 5)	*Vd*
Norway maple	*Acer platanoides*	35 (7 × 5)	*Ap*

The measurements for the species discrimination experiment took place on August 21st and 22nd 2013 from 10:30 to 18:00 local time.

Multispectral and hyperspectral systems in the visible to shortwave infrared (VSWIR; 0.4–2.5 μm) spectral range demonstrated their capability in plant discrimination (Govender et al., 2007; Ustin and Gamon, 2010). This is caused by the fact that the spectral features in the VSWIR are mostly defined by plant constituents such as pigments, leaf water content and other biochemicals like lignin, cellulose (Asner, 1998). Vegetation classification is facilitated by the extraction of distinct and characteristic spectral features in the VSWIR, such as green peak, red edge, and water absorption bands (Asner, 1998; Govender et al., 2007).

While VSWIR spectra have been widely used for many different applications at laboratory to spaceborne levels, the use of the thermal infrared spectral domain (TIR; 8–14 μm) is not as widely spread. The reasons for this are the lack of available spectrometers and the general low SNR in combination with subtle spectral features, which had limited the benefits of TIR spectrometers in the past (Ribeiro da Luz and Crowley, 2007). However, sensor technology has improved in the past years and high resolution spectrometers became available for laboratory, in-situ and even airborne applications. The increasing availability for commercial TIR imaging spectrometers (e.g., Telops HyperCam-LW, Itres TASI-600, Specim AisaOWL) in the last years underline the growing scientific community and the rising number of studies using thermal infrared imaging spectroscopy (Danilina et al., 2012; Vaughan et al., 2003).

Spectral characteristics in the VSWIR consist of combination bands and overtones of primary absorption bands resulting in broad spectral features. As many of the fundamental absorption bands are situated in the TIR region, thermal infrared spectroscopy is assumed to have a large potential for providing complementary information to VSWIR spectroscopy, e.g. identification of vegetation and the quantification of leaf constituents (Ribeiro da Luz, 2006; Silverstein et al., 2005). Despite the general meaning, a few authors demonstrated that vegetation spectra in the TIR are different from blackbody (BB) signatures (Salisbury, 1986; Salisbury and D'Aria, 1992). Moreover, just very recently it could be impressively demonstrated that plant species are discriminable in the TIR (Ribeiro da Luz, 2006; Ullah et al., 2012b). Ullah et al. (2012b) and Fabre et al. (2011) showed that the mid-wave infrared (MWIR; 3–5 μm) is sensitive towards leaf water content and Buitrago et al. (2016) even demonstrated that multiple types of stress could be spectrally identified. These studies were laboratory-based directional hemispherical reflectance (DHR) measurements of single leaves. The results from active DHR spectroscopy can be adapted to passive acquisition techniques used for remote sensing purposes considering Kirchhoff's law. However, these laboratory measurements are time consuming (40 min or longer for each analysis) and only allow for a single, non-imaging leaf measurement at a time (Hecker et al., 2011).

Ribeiro da Luz and Crowley (2007) collected in-situ vegetation emissivity spectra using a passive non-imaging field spectrometer and recognized spectral features identified in laboratory measurements carried out before. Beyond this, new developments in emissive TIR spectroscopy focusing on hyperspectral TIR cameras offer the possibilities for fast and spatial measurements of plant emissivity. Nevertheless, the accuracy of such measurements and their suitability for species discrimination at field conditions has not been tested yet.

2. Objectives

The overall aim of this study was to investigate if plant species discrimination is feasible using emissive TIR imaging spectroscopy. Specific objectives were to: i) compare emissivity spectra from a passive emissive imaging spectrometer with reference spectra from laboratory DHR measurements, ii) classify plant species using the emissivity spectra as input, iii) compare classification accuracies of emissivity spectra with reflectance spectra from a traditional VSWIR spectrometer, iv) demonstrate the ability of identifying spatial heterogeneities using a TIR imaging spectrometer and v) perform a systematic investigation on the effect of SNR on classification results.

3. Methods

During summer 2013, an experiment was carried out in the greenhouse facilities at Trier University. The greenhouse setup allowed plants to be grown under controlled conditions and thermal hyperspectral measurements to be performed next to the greenhouse under clear sky conditions.

3.1. Species discrimination experiment

Eight different plant species were selected for this study (Table 1). Five of the eight species are identical to those used by Ullah et al. (2012b) and represent a wide range of leaves' properties (i.e., colour, thickness, structure, shape) and different canopy structures with expected variations in emissivity. This species setup allows for direct comparison with the results of Ullah et al. (2012b) who assessed plant species discrimination in the thermal spectral region in a laboratory experiment using active DHR spectroscopy.

Seven individual plants from each species were obtained from a local nursery (n = 56). Emissivity measurements of five leaves were taken of each plant, resulting in a total amount of 280 emissivity spectra.

3.2. Thermal infrared

3.2.1. Thermal infrared spectroscopy

Infrared spectroscopy is an analytical technique that is based on vibrational motions within molecules of matters that interact with electromagnetic radiation (Christensen et al., 2000; Hecker et al., 2011). A molecule starts vibrating at fundamental frequency when it is stimulated by absorption of specific electromagnetic radiation. The frequency of such molecular vibration is characteristic for a specific functional group and depends on the atoms' masses and the molecule's geometry. If a molecule absorbs higher amounts of

energy, the molecule is excited in overtones or combinations of fundamental vibration frequencies (Wilson et al., 1955). Whereas NIR and SWIR radiation (0.8–2.5 μm) can excite molecules to overtone vibrations, the midwave and longwave infrared spectral region (2.5–25 μm) may be used to study the fundamental vibrations and associated molecular structures and can be used as a diagnostic tool (Christensen et al., 2000; Salisbury, 1986).

The fundamental vibration frequencies of many constituents composing the superficial epidermal layer of plant leaves are situated in the TIR spectral region. Among others, cellulose, hemicellulose, varieties of pectin and aromatic compounds have characteristic features in the 8–2 μm spectral range (Elvidge, 1988; Ribeiro da Luz and Crowley, 2007; Riederer and Muller, 2006; Ullah et al., 2012a). This is why TIR spectroscopy is assumed to have large potential for identification of species specific surface compositions and species discrimination.

While several techniques allow the acquisition of thermal infrared spectroscopy data, this study focuses on a passive acquisition technique. Passive measurements of emitted thermal infrared radiation always require a thermal contrast between the sample and the environment to distinguish the sample signal from radiation emitted from surroundings such as walls, ceilings, buildings and instruments, which is reflected by a surface different from a blackbody. When measuring inside a laboratory, the sample needs to be heated up to at least 20 K above ambient temperature to produce this thermal contrast (King et al., 2004; Salisbury and D'Aria, 1994; Schlerf et al., 2012). This method is not suitable for green leaves and other temperature sensitive samples. Alternatively, thermal measurements are possible outside under clear sky conditions. The relatively poor downwelling radiation (DWR) from clear sky appears like radiation emitted from a very cold blackbody and the samples can be measured at ambient temperature. The sample should be isolated from radiating objects, because the high amount of radiation from warm objects would overpower the subtle spectral contrast of plant spectra.

3.2.2. Measurement setup

Hyperspectral thermal infrared imaging data were collected using a HyperCam-LW (Telops Inc., Québec, Canada) camera that measures radiation emitted from objects in many narrow bands. This instrument is a Fourier-transform imaging spectrometer, using a 320 × 256 pixel MCT (mercury cadmium telluride) detector and records one interferogram per pixel. TIR radiance spectra can be derived from these interferograms at a spectral resolution of up to 0.25 cm^{-1} (Schlerf et al., 2012). To prevent disturbances by self-emission, the detector is cooled down to 65 K. The spectrometer was equipped with a wide-angle telescope and a 45° tilted gold-coated mirror, which allows a vertical view with a field of view of 25.6° × 30.6 °corresponding to 443 mm × 358 mm and a pixel size of 2.07 mm at 1.5 m distance. A spectral sampling distance of 3.3 cm^{-1} with 4 cm^{-1} FWHM (Full Width at Half Maximum) corresponding to 40 nm at 10 μm was chosen in the spectral domain from 865 to 1280 cm^{-1} (7.8–11.56 μm), resulting in 125 bands.

At a distance of 1.5 m, a highly diffuse reference target (Infragold®, Labsphere Inc, North Sutton, USA) of known reflectance was centred in the scans to quantify DWR. Five leaves were picked per plant and clipped in a sample holder in front just above the Infragold® panel. This setup allowed the acquisition of image cubes only composed of sample spectra and DWR. Another advantage of this setup is that target and background spectra are clearly different and this allows the identification of mixed leaf border pixel. Most of the spectrometer and the tripod were covered by crinkled aluminium foil to avoid thermal radiation emitted from the equipment from disturbing the measurements.

To achieve a high signal-to-noise ratio (SNR), eight consecutive acquisitions were collected per scene. One acquisition taking eight seconds, the total acquisition time was about one minute per scene. Because of subtle temperature fluctuations due to wind, these eight single data cubes were individually processed before being averaged.

3.2.3. Image processing and temperature-emissivity separation

The radiometric calibration interferogram datacubes, including Fourier transformation, 2-point-blackbody calibration (BB_{cold} = 20 °C and BB_{hot} = 35 °C) and bad pixel correction, was accomplished using the *Reveal Calibrate* software (Telops, Quebec, Canada). A Hamming windowing function was chosen as apodization window, resulting in smooth radiance spectra (Blackman and Tukey, 1958).

The resulting radiance datacubes were then processed to spectral emissivity. The self-emission of an object at some temperature T is modulated by the emissivity of the material. In addition, for surfaces with emissivities differing from unity, the object leaving radiance contains a reflected downwelling component from the atmosphere. This DWR not only originates from the atmosphere above the sample, but also from the surrounding objects, such as equipment and buildings. On the other hand, the intervening atmosphere absorbs some of the surface leaving radiance and adds path radiance. Thus, the hyperspectral TIR spectra need to be corrected for these effects to retrieve surface emissivity and temperature. This is commonly combined in a process known as temperature and emissivity separation (TES).

DWR spectra, measured using an Infragold® plate, need to be corrected for the plate's self-emission that requires knowing the temperature and emissivity of the reference targets. For the Infragold® target an average emissivity of 0.046 in TIR was gathered from the calibration certificate, and the Infragold® temperature was assumed to be ambient temperature.

When DWR is known, surface emissivity spectrum is derived using the following equation:

$$\varepsilon_S(\lambda) = \frac{L_S(\lambda) - L_{DWR}(\lambda)}{L_{BB}(T_S, \lambda) - L_{DWR}(\lambda)} \quad (1)$$

where $\varepsilon_S(\lambda)$ is the sample's spectral emissivity, $L_{DWR}(\lambda)$ the downwelling radiance, and $L_{BB}(T_S, \lambda)$ the blackbody radiance at the sample's kinetic temperature T_S. In order to use Eq. (1), exact knowledge of the sample kinetic temperature is required.

Since kinetic surface temperatures are typically not known with the required accuracy, alternative processing approaches have to be used. For temperature retrieval under clear sky conditions, the "Downwelling Radiance Residual Index (DRRI)"- method (Wang et al., 2008) was chosen, which is based on the "spectral smoothness" – approach (Horton et al., 1998). Although this method is only applicable under clear sky conditions, it is less restrictive than the "reference channel" – approach (Kahle and Alley, 1992) and the "maximum spectral temperature" – approach (Korb et al., 1996) because it requires no a priori knowledge (e.g. peak value of emissivity, wavelength of peak emissivity). The sole premise of the DRRI approach is that the distance from sample to sensor is very short and that atmospheric contribution is negligible within this path.

For the application of the DRRI approach, DWR and the surface leaving radiance (approximated here by the radiance at sensor) need to be known. This data being extracted from the hyperspectral thermal infrared image data, the remaining surface temperature and surface emissivity is derived by an optimization algorithm, trying to find the surface temperature which is the solution for DRRI = 0 (OuYang et al., 2010).

3.2.4. Validation of emissivity spectra

For validation, HyperCam-LW spectra were compared to reference spectra from a laboratory spectrometer. Reference measurements were done at the spectroscopic facilities of the Uni-

versity of Twente's GeoScience Laboratory using a Bruker Vertex 70 FTIR laboratory spectrometer, equipped with an integrating sphere (Hecker et al., 2011). For every species, one representative plant was selected and 5 leaves were picked for reference measurements. Checking the range of the absolute values and the remaining atmospheric residual peaks in the processed spectra provides good initial information on the quality of the applied TES. This first test was consolidated by the calculation of similarity criteria such as the Pearson's correlation coefficient (r) and the Nash-Sutcliff-Efficiency index (NSE) (Nash and Sutcliffe, 1970). The NSE ranges from 1 to $-\infty$ where NSE < 0 indicates that the mean value of the HyperCam-LW spectrum would have been a better predictor than the HyperCam-LW spectrum, NSE > 0 indicates that the HyperCam-LW spectrum performs better than the mean value and NSE = 1 corresponds to a perfect match between HyperCam-LW spectra and Bruker reference measurements. For each species, 100 image pixels were randomly selected over all leaves for comparison with one average reference spectrum. From these values, the probability density function was derived and the mode of this function was used to characterize the most representative similarity value between the HyperCam-LW spectra and Bruker reference spectra.

3.3. Visible to shortwave infrared

To compare the separation power for species discrimination using TIR data to that of traditional VSWIR spectra, we collected additional spectra in the 350–2500 nm spectral range using an ASD FieldSpec® III spectroradiometer (Analytical Spectral Devices Inc., Boulder, CO, USA) equipped with a Plant Probe. The Plant Probe consists of a clamp with a constant light source and a rotating dark or white background with a spot size diameter of 10 mm. This setup allows for non-destructive leaf measurements under controlled illumination conditions (Carvalho et al., 2013). Immediately after the hyperspectral thermal infrared measurements, the same five leaves per plant were measured individually in the reflective domain. The spectroradiometer was calibrated using the white reference target of the leaf-clip. In order to derive leaf surface reflectance, the single leaves were clamped in front of the black background of the leaf-clip. For every leaf, three leaf-clip measurement were distributed of the central part of the leaves, each averaged over 30 single measurements. These 90 spectra were averaged resulting in one spectrum per leaf representing an area of approximately 240 mm^2. White reference and grating drift corrections were performed on each spectrum following Dorigo et al. (2006) As a result, 280 reflectance spectra were collected in the VSWIR spectral domain and used further for the statistical analysis.

3.4. Statistical analysis

A Random-Forest classifier (RFC) (Breiman, 2001) was chosen for species classification. This classifier is non-parametric and is well suited to analyse high dimensional data. For statistical analysis, spectral bands dominated by water vapour from 7.8 μm–8.037 μm were removed from the spectra, resulting in a spectral range of 865 cm^{-1}–1244 cm^{-1} (8.038–11.56 μm) for the TIR and 400 nm–2450 nm for the VSWIR.

3.4.1. Comparison of discrimination accuracies in different spectral ranges

Since the same leaves were measured in the TIR and VSWIR spectral range, a comparison of classification accuracies could be accomplished. For the VSWIR spectral range, the averaged 280 reflectance spectra were subjected to the RFC. To make the TIR dataset comparable to the VSWIR dataset, the TIR image data were reduced to one emissivity spectrum per leaf by averaging 20 random pixel from the image dataset, covering the same area as the VSWIR spectrometer's plant probe. The resulting 280 emissivity spectra were subjected to the RFC. To assess the heterogeneity of the dataset, averaging of emissivity pixel followed by RFC was performed 20 times. To select the most representative classification model from the 20 individual classification runs, quality measures like OAA and Kappa values were recorded. From these values, the probability density function was derived and the mode of this function was used to characterize the classification accuracy.

3.4.2. Image classification

For image classification 100 pixels per species were randomly selected as training dataset and another set of 100 different pixels were randomly selected as validation dataset. To account for the effects of pseudoreplication on the classification accuracy, which arises from the fact that each five leaves were picked from the same plant, training data were collected from 4 of the 7 individual plants and validation data from the remaining 3 plants. The image background consisting of an Infragold® reference plate was used as an additional endmember into the discrimination analysis. For the RFC a data reduction was carried out using a principal component analysis (PCA). The number of principal components was chosen to reach a cumulative proportion of > 0.95. As in 3.4.1., 20 classification runs were performed. To select the most representative classification model, the classification model closest to the mode of the OAA density function was selected. This most representative model was applied to the image dataset.

To investigate the influence of SNR on the classification results, the methodology described above was applied on two additional datasets: Before being subjected to TES, the radiance datasets were preprocessed with i) a 3×3 kernel filter and ii) a 5×5 kernel filter. In order to avoid averaging of leaf and background pixel at the edges of leaves, a median filter was chosen as kernel filter.

3.4.3. Spectral band reduction

To assess the importance of certain wavebands for species discrimination, the random forest classifier's band importance was derived. Band importance is determined as the mean decrease in accuracy (MDA) during processing, i.e. the difference in prediction accuracy, averaged over all trees, before and after randomly permuting the predictor variable and breaking its original association with the response (Breiman, 2001; Nicodemus, 2011). Further, to investigate the predictive power of the most important bands, classification was repeated with an increasing number of input bands, selected by decreasing importance.

4. Results

4.1. Visible to shortwave infrared

Focusing on the spectral signatures in the VSWIR, the shapes of the spectra only show small between-species variabilities. Spectral behaviour of all species is clearly determined by common features, such as green peak, pigment absorption minima, red edge, infrared plateau with minor water absorption bands, and SWIR with major water absorption bands. In the NIR all the species present an average maximum reflectance between 44% and 52%, with the exception of *Acer platanoides* which shows significantly lower reflectance values (Fig. 1). Looking into detail, the standard deviation of *Liquidambar styraciflua* and *Ginkgo biloba* is significantly larger in comparison to the remaining 6 species due to differences in leaf structure.

4.2. Validation of emissivity spectra

A first visual evaluation of the emissivity spectra presents smooth signatures in a rational range. Fig. 2 shows the spectral

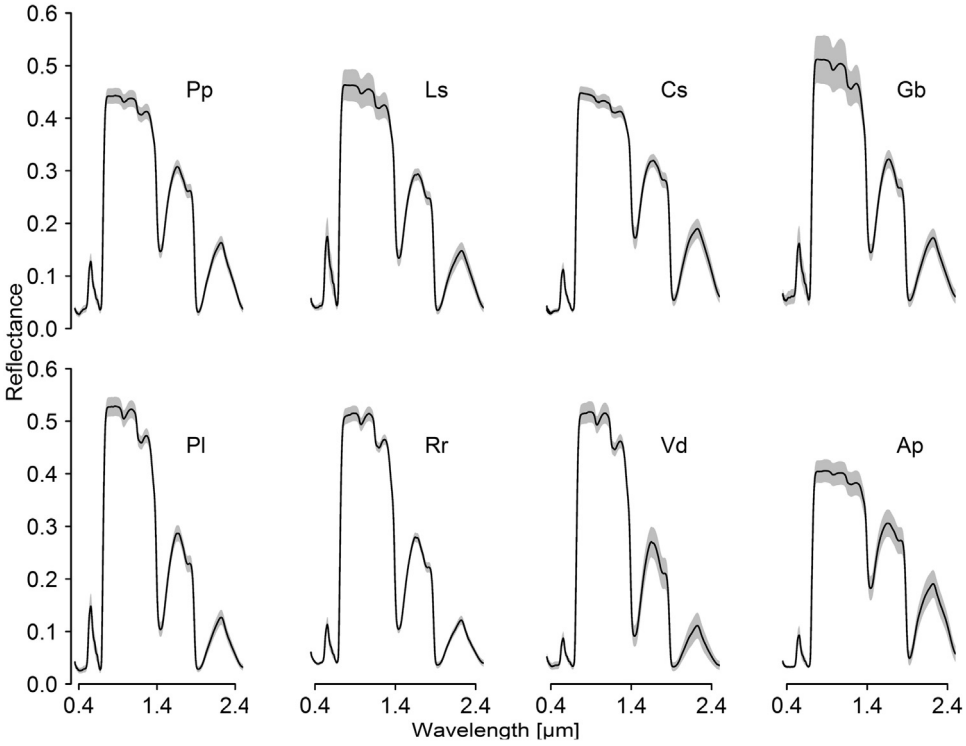

Fig. 1. VSWIR spectra for the investigated species. Black: Mean spectra (N = 35), grey: mean +/− 1 standard deviation.

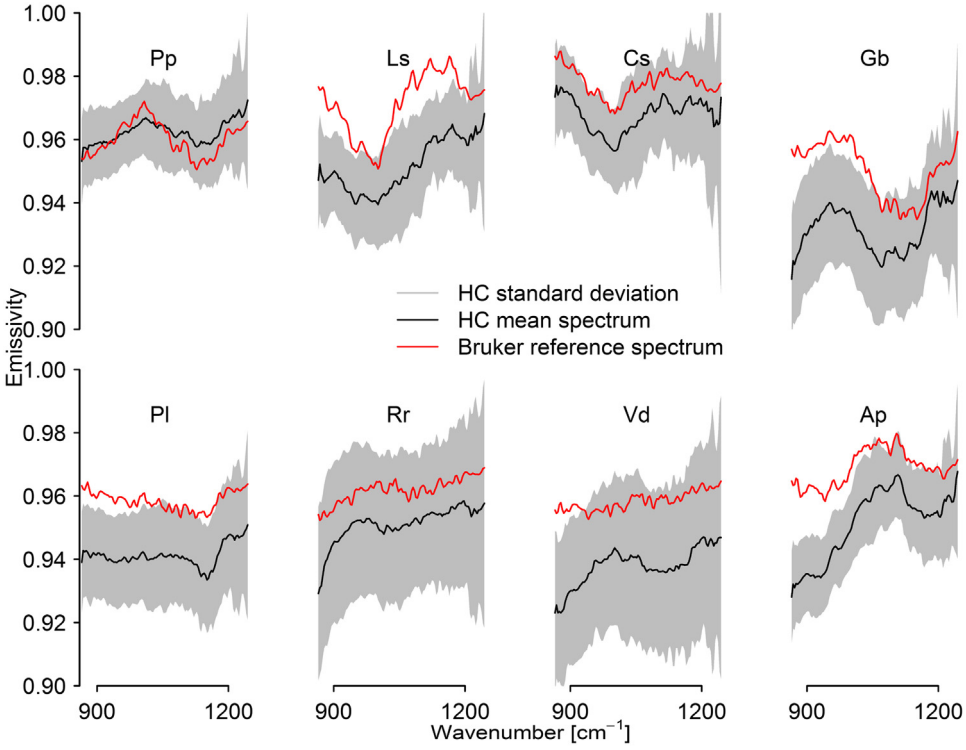

Fig. 2. Comparison of HyperCam-LW spectra (black line: average of 100 randomly selected pixel, grey: mean +/− 1 sd) with Bruker reference spectra (red line). (For interpretation of the references to colour in this figure legend, the reader is referred to the web version of this article.).

information per species. The different vegetation spectra, with a range of emissivity from 90% to 99% show distinctive shapes comprising mainly a low frequency component superimposed by a variety of narrow spectral features. Although an offset between HyperCam-LW and the reference spectra is present for large parts of the spectral range, the shapes of the spectra correspond relatively well to the reference spectra. The offset varies from 1 to 3% (absolute emissivity) for different species.

To remove the offset between HyperCam-LW spectra and reference spectra for a better comparison of their shapes, vector

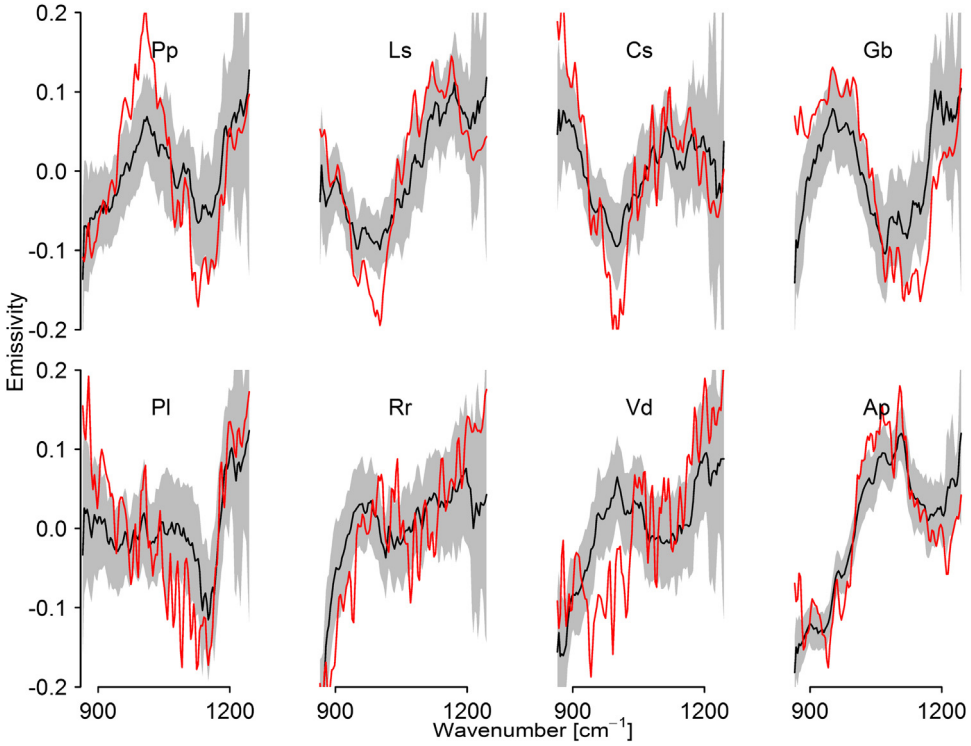

Fig. 3. Comparison of vector normalized HyperCam-LW spectra (grey and black) and Bruker reference spectra (red). (For interpretation of the references to colour in this figure legend, the reader is referred to the web version of this article.)

Table 2
Nash-Sutcliffe-Efficiency Index (NSE) and Pearson's correlation coefficient (r) for the different species measured with the HyperCam-LW and Bruker Vertex 70.

Species	r	NSE	
Prunus persica	0.958	0.78	+++
Liquidambar styraciflua	0.943	0.73	++
Cornus sericea	0.913	0.63	++
Ginkgo biloba	0.778	0.58	++
Prunus lauracerasus	0.757	0.50	+
Rhododendron repens	0.841	0.65	++
Viburnum davidii	0.681	0.44	+
Acer platanoides	0.927	0.84	+++

Table 3
Classification results (mode +/− 1 sd of 20 classification runs) for the two spectral domains.

Spectral Range	OAA	kappa
TIR	92.26% (+/− 1.54)	0.9115 (+/− 0.0176)
VSWIR	80.28% (+/− 0.43)	0.7746 (+/− 0.0049)

normalization was applied. Normalization is performed by dividing the single band's values by the sum of all of the 115 band values. Fig. 3 shows normalized spectra. In general, the overall shape of HyperCam-LW spectra fit well to the normalized reference spectra.

The similarity values (NSE and r) between normalized HyperCam-LW spectra and Bruker reference spectra are listed in Table 2. All of the tested species have positive NSE of which five have NSE values > 0.60. While *Acer platanoides* and *Prunus persica* present the best results, *Ginkgo biloba*, *Viburnum davidii* and *Prunus lauracerasus* present the poorest. These results support the visual analysis of the image data (Fig. 4).

4.3. Species discrimination

4.3.1. Comparison of discrimination accuracies in different spectral ranges

The results shown in Table 3 compare the classification results of TIR spectral range with respect to the reflective spectral range. While Table 3 presents the overall accuracies for both spectral domains, Tables 4 and 5 present the error matrix allowing an in-depth analysis of the results.

Classification results based on thermal infrared spectroscopy data outperform the classifications based on VSWIR data by almost 12% in OAA.

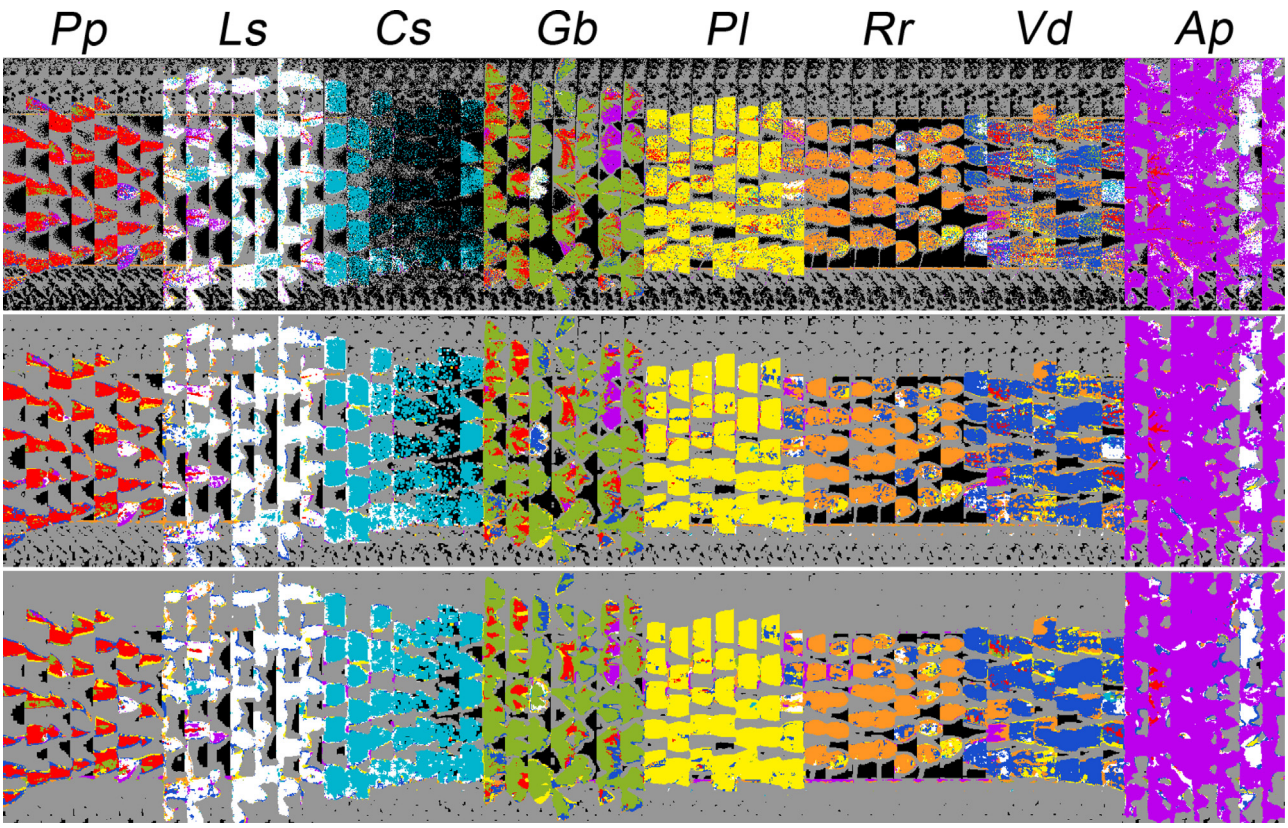

Fig. 4. Classification result from native spatial resolution (top), 3 × 3 spatial averaging (middle) and 5 × 5 spatial averaging (bottom). Colour: species, grey: background, black: pixel with non-converging TES. The 5 leaves from one column originate from one plant. The leaves from Ap being much larger than the remaining, it seems that a lot of background pixel were misclassified, which is not the case.

Table 4
representative error matrix for a single classification run based on TIR spectroscopy data.

		Reference data									
		Pp	*Ls*	*Cs*	*Gb*	*Pl*	*Rr*	*Vd*	*Ap*	Total	User's Accuracy [%]
Classification	*Pp*	**31**	5	0	0	0	0	0	0	36	86.11
Results	*Ls*	3	**30**	0	0	0	0	0	0	33	90.91
	Cs	0	0	**35**	0	1	0	0	0	36	97.22
	Gb	1	0	0	**31**	4	0	0	0	36	86.11
	Pl	0	0	0	4	**30**	0	0	0	34	88.24
	Rr	0	0	0	0	0	**34**	1	0	35	97.14
	Vd	0	0	0	0	0	1	**33**	1	35	94.29
	Ap	0	0	0	0	0	0	1	**34**	35	**97.14**
Total		35	35	35	35	35	35	35	35	280	
Producer's Accuracy [%]		88.57	85.71	100.00	88.57	85.71	97.14	94.29	97.14	Overall Accuracy: 92.14% Kappa statistic: 0.9102	

Table 5
representative error matrix for a single classification run based on VSWIR spectroscopy data.

		Reference data									
		Pp	*Ls*	*Cs*	*Gb*	*Pl*	*Rr*	*Vd*	*Ap*	Total	User's Accuracy [%]
Classification	*Pp*	**29**	7	3	0	0	0	0	0	36	74.36
Results	*Ls*	2	**22**	0	2	2	0	0	0	33	78.57
	Cs	2	0	**30**	2	2	0	1	9	36	68.18
	Gb	0	3	0	**31**	2	0	0	0	36	91.18
	Pl	0	3	0	0	**30**	1	1	0	34	85.71
	Rr	0	0	0	0	1	**29**	5	0	35	82.86
	Vd	0	0	0	0	2	5	**27**	0	35	79.41
	Ap	2	0	2	0	0	0	0	**26**	35	86.67
Total		35	35	35	35	35	35	35	35	280	
Producer's Accuracy [%]		82.86	62.86	85.71	88.57	85.71	82.86	79.41	74.29	Overall Accuracy: 80.29% Kappa statistic: 0.7747	

Table 6
Error matrix from classification result based on native spatial resolution image data.

		Reference data										
		Pp	*Ls*	*Cs*	*Gb*	*Pl*	*Rr*	*Vd*	*Ap*	bgrd	Total	User's Accuracy [%]
Classification	*Pp*	**53**	1	0	12	7	0	10	5	0	88	60.2
Results	*Ls*	0	**81**	10	0	0	2	1	10	9	113	71.7
	Cs	1	5	**87**	1	7	7	5	0	5	118	73.7
	Gb	12	0	0	**68**	2	0	1	0	0	83	81.9
	Pl	7	1	1	2	**74**	4	8	0	2	99	74.7
	Rr	0	0	0	3	3	**74**	23	0	2	105	70.5
	Vd	7	1	0	5	5	7	**38**	0	1	64	59.4
	Ap	18	10	0	8	1	0	9	**82**	2	130	63.1
	bgrd	2	1	2	1	1	6	5	3	**79**	100	**79.0**
Total		100	100	100	100	100	100	100	100	100	900	
Producer's Accuracy [%]		53.0	81.0	87.0	68.0	74.0	74.0	38.0	82.0	79.0	Overall Accuracy: 70.7%	
											Kappa statistic: 0.67	

Table 7
Error matrix from classification result based on spatial averaged (3 × 3) image data.

		Reference data										
		Pp	*Ls*	*Cs*	*Gb*	*Pl*	*Rr*	*Vd*	*Ap*	bgrd	Total	User's Accuracy [%]
Classification	*Pp*	**81**	2	0	9	3	0	3	1	0	99	81.8
Results	*Ls*	0	**91**	4	0	0	0	0	8	0	103	88.3
	Cs	0	3	**96**	0	0	0	0	0	3	102	94.1
	Gb	4	1	0	**71**	0	0	0	0	0	76	93.4
	Pl	5	0	0	1	**95**	5	1	1	1	109	87.2
	Rr	0	0	0	0	0	**85**	23	0	2	110	77.3
	Vd	2	0	0	4	2	8	**69**	3	1	89	77.5
	Ap	6	3	0	15	0	0	2	**87**	2	115	75.7
	bgr	2	0	0	0	0	2	2	0	**91**	97	**93.8**
Total		100	100	100	100	100	100	100	100	100	900	
Producer's Accuracy [%]		81.0	91.0	96.0	71.0	95.0	85.0	69.0	87.0	91.0	Overall Accuracy: 85.11%	
											Kappa statistic: 0.8325	

Table 8
Error matrix from classification result based on spatially averaged (5 × 5) image data.

		Reference data										
		Pp	*Ls*	*Cs*	*Gb*	*Pl*	*Rr*	*Vd*	*Ap*	bgrd	Total	User's Accuracy [%]
Classification	*Pp*	***85***	*1*	*0*	*11*	*0*	*0*	*0*	*2*	0	121	85.9
Results	*Ls*	1	**90**	6	0	0	0	0	4	2	115	87.4
	Cs	0	2	**92**	0	0	1	0	0	2	105	94.8
	Gb	4	0	0	**79**	0	0	0	0	0	83	95.2
	Pl	0	1	0	0	**95**	4	1	0	1	114	93.1
	Rr	0	0	0	0	0	**88**	4	0	0	78	95.7
	Vd	0	0	0	1	5	5	**92**	1	0	79	88.5
	Ap	10	6	0	9	0	0	2	**93**	1	106	76.9
	bgrd	0	0	2	0	0	2	1	0	**94**	99	94.9
Total		100	100	100	100	100	100	100	100	100	900	
Producer's Accuracy [%]		85.0	90.0	92.0	79.0	95.0	88.0	92.0	93.0	94.0	Overall Accuracy: 89.8%	
											Kappa statistic: 0.8850	

4.3.2. Image classification

Tables 6–8 show the classification results of TIR image data for different spatial smoothing pre-processings (native spatial resolution (Table 6), 3 × 3 (Table 7) and 5 × 5 (Table 8) averaging window).

The classification of thermal spectroscopic image data at full spatial resolution achieved an OAA of 70.7% (Kappa = 0.67) which indicates a good overall discrimination of the investigated plant species using emissivity spectra. These accuracies rise with increasing averaging window size (3 × 3 averaging: OAA = 85.1%, Kappa = 0.83; 5 × 5 averaging: OAA = 89.8%, Kappa = 0.89).

Consistently, for classifications of the three image datasets, *Pp*, *Gb* and *Vd* show the poorest results. Mostly, *Pp* is confused with *Gb* and *Ap*, *Gb* is confused with *Pp* and *Ap* and *Vd* is confused with *Pp* and *Rr*. While these three species are often confused with *Ap*, the latter is classified with high accuracies.

Image classification results depicted in Fig. 4 show a good performance in general. Most of the leave pixels were correctly assigned. Misclassifications mostly occurred on complete leaves or certain parts of leaves. The leaves of *Cornus sericea* comprise a high percentage of NA-values (black pixels), which results from a non-converging of the residual minimizing algorithm during TES. Except for the NA-values, *Cornus sericea* does not show many misclassifications. For *Acer platanoides* large parts of leaves originating from one single plant show a high percentage of misclassifications, which could be due to intraclass variability. While *Ginkgo biloba* is mostly confused with *Prunus persica* and *Acer platanoides, Viburnum davidii* is confused with most of the remaining classes (i.e. *Prunus persica, Liquidambar styraciflua, Cornus sericea, Prunus lauroacerasus, Rhododendron repens* and *Acer platanoides*). All other species mostly present random misclassifications with remaining species.

With increasing SNR (Fig. 4 middle and bottom), the number of misclassification is strongly reduced and only coherent misclassifications remain in the resulting image. This points to the spatial heterogeneity in individual leaves.

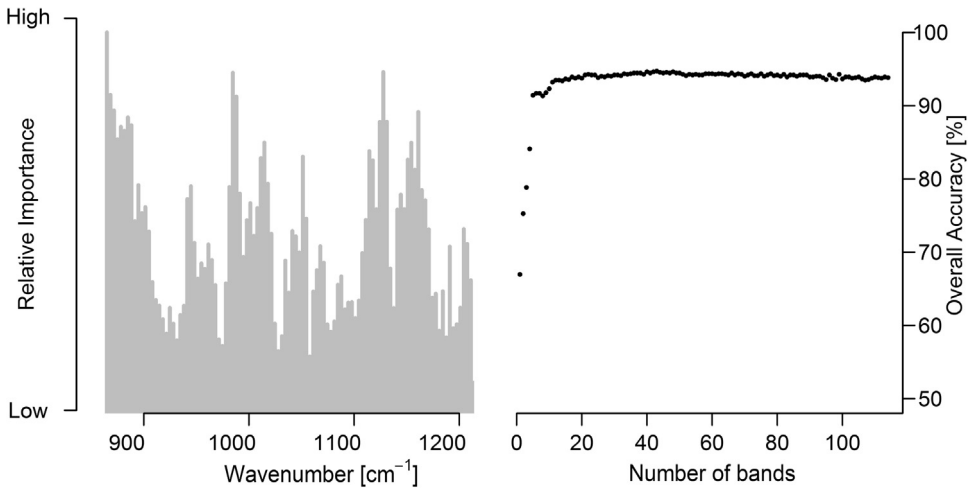

Fig. 5. Relative importance of spectral band for RFC (left) and OAA of RFC by increasing number of spectral bands (right).

4.3.3. Spectral band reduction

Fig. 5 depicts the relative importance of spectral band for discrimination of the 8 species (left) and the accuracies achieved during classification using an increasing number of spectral bands with respect to their importance (right). Local maxima and minima (8.19 μm/1220.90 cm^{-1}, 8.4 μm/1190.96 cm^{-1}, 8.49 μm/1177.65 cm^{-1}, 9.7 μm/1031.28 cm^{-1}, 10.19 μm/981.38 cm^{-1}, 10.51 μm/951.44 cm^{-1}, 10.81 μm/924.82 cm^{-1}) in band importance agree well with results from Ullah et al. (2012b). The discrimination accuracy varies with respect to the number of bands used for classification. Starting from an OAA of 66.94% for 2 bands, the discrimination accuracy increases up to 91.79% for 6 bands. Further increase of bands leads to a weak gain in accuracy up to 94.73% for 44 spectral bands (Fig. 5, right). These results fit well with the results from the comparison of classification accuracies for different spectral ranges (Tables 4 & 5).

5. Discussion

Data acquisition using a hyperspectral thermal infrared camera (such as the Telops HyperCam-LW) is a fast and accurate way of measuring emissivity spectra of plants in a spatially continuous way. As multiple pixels can be averaged for homogeneous samples, SNR increases and derived emissivity spectra compare well to laboratory reference spectra.

When comparing the HyperCam-LW spectra with laboratory reference spectra, an offset of 1–3% (absolute emissivity) was detected. This offset can have various reasons: i) errors in the temperature estimation during TES or ii) the radiometric calibration or iii) systematic spectrometer errors. Since the HyperCam-LW spectra presented smooth shapes and did not show any large atmospheric residuals, errors during TES and radiometric calibration could be excluded. Hecker et al. (2011) conclude that the described Bruker FTIR laboratory spectrometer tends to have marginally lower values at very low reflectance in comparison to similar spectrometers. Therefore, lower reflectance corresponding to higher emissivity values would explain the offset in vegetation spectra, usually ranging between 94–99% of emissivity or 1–6% of reflectance. This offset was eliminated by vector normalization in both datasets to allow the shapes of the emissivity curves to be compared.

When looking very closely at the different spectra, small divergences are still detectable between HyperCam-LW and Bruker reference spectra. The reason for these divergences is probably related to the fact that the acquisition of reference measurements could not be taken simultaneously with the HyperCam-LW measurements and leaves that were picked for both measurements were not identical.

The DRRI approach to derive emissivity from radiance data appears to be a well-suited TES method for field measurements at short distances from the sample. Minimizing an average smoothness value is affected by noise and leads to atmospheric residuals in the resulting emissivity spectrum. This is why our temperature retrieval focused on minimizing residuals of the most prominent water line, i.e. the line at 1174.53 cm^{-1} (8.514 μm), which is included in the spectral band with centre wavenumber 1174.33 cm^{-1} (8.515 μm). The fact that the remaining residuals in the individual spectra are compensated by averaging multiple pixels per leaf illustrates that the TES algorithm has a good performance and does not produce a systematic over- or underestimation of temperature.

Concerning intraclass heterogeneity, especially the spread of the *Rhododendron repens* and *Viburnum davidii* spectra is wider than for the remaining species (Fig. 2). As the samples were randomly chosen within one canopy, leaves of different ages and illumination conditions, presenting different physiological and biochemical conditions, were selected, resulting in different spectral emissivities (Buitrago et al., 2016).

Species discrimination using a random forest classifier led to good results and improved significantly with respect to spatial averaging. In summary, the initial dataset achieved an OAA of 70.7%, the 3×3 averaging pre-processing resulted in an OAA of 85.1% and the 5×5 averaging pre-processing in an OAA of 89.8%. On the whole, TIR spectroscopy allows for identification of objects with very subtle spectral signatures and differences. With reference to Fig. 4, the consistent confusions of *Pp* and *Gb* spectra are related to the similarity of the species specific spectra. The misclassifications of many pixel as *Vd* are due to the wide variance within the species spectra. The lower variance and the unique spectral shape for *Ap* causes the good producer's accuracy (93.0%) and the corresponding poorer user's accuracy (76.9%).

Misclassifications are not distributed randomly over the complete dataset but concentrate on complete or certain parts of leaves. It appears that this is related to a spatial variation of emissivity spectra caused by inhomogeneity of biochemistry and leaf structural properties within and between leaves of the same species. Especially some leaves from *Ginkgo biloba* present misclassifications at the apexes and all the leaves from one *Acer platanoides* plant present wide misclassifications. This fact points to the assumption that the

leaves and some individual plants were in different physiological states, i.e. showed signs of stresses. The identification of these spatial heterogeneities impressively demonstrates the advantage of imaging over non-imaging spectroscopy.

In order to provide a complete impression on the potential of the Telops HyperCam-LW, classification was also performed on single measurements. The results are poorer than those obtained from image datasets averaged over eight repeated measurements (Tables 6–8) but, even with single measurements, OAA of 54.67% could be achieved. With spatial averaging pre-processing OAA of 65.67% and 76.11% were achieved for kernel sizes of 3×3 and 5×5 respectively.

Comparing with a laboratory study from Ullah et al. (Ullah et al., 2012b) who achieved an OAA of 92%, these results are completely satisfying, taking into account the argument of an in-situ experiment, the smaller spectral range and the very short duration per acquisition.

These classification results confirm the stated hypothesis, which means that TIR measurements are well suited for vegetation analysis. In addition, these results confirm that for this special experimental setup, hyperspectral thermal infrared measurements provide better classification results than measurements in the reflective domain. This can be explained by the fact that primary absorption bands of many constituents are located in the TIR spectral region.

The results of the band reduction experiment meet our expectations. Selecting single narrow bands, with respect to their importance during classification, indicated a significant improvement of OAA when selecting up to 6 bands. Adding more bands to the classification did only result in a slight improvement for classification results. Although these results are remarkable and would lead to a conclusion that a sensor comprising only 6–10 well-chosen bands would allow for similar results, it needs careful evaluation. Obviously, the considered plants differ more with respect to their spectral emissivity shapes than the respective reflectance curves in the solar spectral domain. However, without further studies, this result cannot be generalized to other plant species, which might have similar spectral characteristics in the TIR but unique features in the VSWIR.

Though at near range, TIR imaging spectroscopy allows for accurate and reliable retrieval of plant emissivities and species discrimination, there are still many challenges to overcome for airborne and future spaceborne sensors: 1. Atmosphere correction and TES algorithms require knowledge of the spatial distribution of atmospheric water vapour. Its quantification requires radiance measurements in narrow spectral bands which are generally limited in their signal to noise ratio. 2. Increasing observation distances implies scale effects related to structural issues (i.e. mixed pixels, scattering, re-radiation and cavity effects) (Kirkland et al., 2002) resulting in non-linear mixtures of signatures and reduction of spectral contrast (Gillespie, 1992; Ribeiro da Luz and Crowley, 2010).

6. Conclusion

This study demonstrated the suitability of the TIR spectral range for species discrimination. Important aspects of the study include i) that the suitability of the Telops HyperCam-LW for TIR data acquisition does not only account for gases, but for surfaces of low spectral contrast, too, ii) the ability of discriminating multiple plant species using emissive imaging spectroscopy, iii) the superiority of emissivity spectra over VSWIR reflectance data for this special experimental setup, iv) the ability to uncover spatial heterogeneities using the TIR imaging spectrometer, and v) the influence of SNR on the classification results.

In our experiment we demonstrated that the Telops HyperCam-LW is not only suitable for data acquisition of samples with very prominent spectral features, e.g. gas detection purposes or mineral detection (Schlerf et al., 2012), but, in addition, is able to collect high-quality data suitable for surface analysis for materials with very subtle spectral signatures, such as vegetation.

Further, we showed that the TIR spectral range is suitable for species discrimination. Although, the spectral contrast for vegetation in the TIR only spans 4% absolute emissivity, the spectral signatures of the selected species show substantial differences in shape, which is different from the reflective spectral domain. Therefore, TIR spectroscopy can be considered as a valuable addition to VSWIR spectroscopy for vegetation studies. As the spectral contrast is relatively low, an increase in SNR has a positive effect on classification results.

Finally, we demonstrated that emissive TIR imaging spectroscopy provides fast measurements and accurate as well as reliable results, comparable to laboratory spectrometers. In addition, TIR imaging spectroscopy offers the ability to uncover spatial distributions of surface properties, usually hidden during laboratory non-imaging studies.

Acknowledgements

The authors wish to thank the Fonds National de la Recherche (FNR) of Luxembourg for funding the PhD research of Gilles Rock [AFR reference: 2011-2/SR/2962130] and the PLANTSENS research project [AFR reference: C13/SR/5894876]. In addition the authors would like to thank Trier University's department for Geobotany and the ITC (University of Twente, the Netherlands) for the use of their equipment and facilities. Finally, a special thank goes to Christian Bossung, Henning Buddenbaum, Kim Fischer, Thomas Gattung, Miriam Machwitz and Franz Kai Ronellenfitsch for their tireless support during the experiment.

References

Asner, G.P., 1998. Biophysical and biochemical sources of variability in canopy reflectance. Remote Sens. Environ. 64, 234–253, http://dx.doi.org/10.1016/S0034-4257(98)00014-5.

Blackman, R.B., Tukey, J.W., 1958. The measurement of power spectra from the point of view of communications engineering. Bell Syst. Tech. J. N. Y.: Dover, http://dx.doi.org/10.1002/j.1538-7305.1958.tb03874.x.

Breiman, L., 2001. Random forests. Mach. Learn. 45, 5–32, http://dx.doi.org/10.1023/A:1010933404324.

Buitrago, M.F., Groen, T.A., Hecker, C.A., Skidmore, A.K., 2016. Changes in thermal infrared spectra of plants caused by temperature and water stress water stress. ISPRS J. Photogramm. Remote Sens. 111, 22–31, http://dx.doi.org/10.1016/j.isprsjprs.2015.11.003.

Carvalho, S., Schlerf, M., van der Puttena, W.H., Skidmore, A.K., 2013. Hyperspectral reflectance of leaves and flowers of an outbreak species discriminates season and successional stage of vegetation. Int. J. Appl. Earth Obs. Geoinf. 24, 32–41, http://dx.doi.org/10.1016/j.jag.2013.01.005.

Christensen, P.R., Bandfield, J.L., Hamilton, V.E., Howard, D. a., Lane, M.D., Piatek, J.L., Ruff, S.W., Stefanov, W.L., 2000. A thermal emission spectral library of rock-forming minerals. J. Geophys. Res. 105, 9735–9739, http://dx.doi.org/10.1029/1998JE000624.

Danilina, I., Gillespie, A.R., Balick, L.K., Mushkin, A., O'Neal, M. a., 2012. Performance of a thermal-infrared radiosity and heat-diffusion model for estimating sub-pixel radiant temperatures over the course of a day. Remote Sens. Environ. 124, 492–501, http://dx.doi.org/10.1016/j.rse.2012.05.028.

Dorigo, W., Bachmann, M., Heldens, W., 2006. AS Toolbox & Processing of Field Spectra, User's Manual. German Aerospace Center (DLR), Oberpfaffenhofen, 82234, Wessling, Germany.

Elvidge, C.D., 1988. Thermal infrared reflectance of dry plant materials: 2.5–20.0 μm. Remote Sens. Environ. 26, 265–285, http://dx.doi.org/10.1016/0034-4257(88)90082-X.

Fabre, S., Lesaignoux, A., Olioso, A., Briottet, X., 2011. Influence of water content on spectral reflectance of leaves in the 3–15-μm domain. IEEE Geosci. Remote Sens. Lett. 8, 143–147, http://dx.doi.org/10.1109/LGRS.2010.2053518.

Gillespie, A.A.R., 1992. Spectral mixture analysis of multispectral thermal infrared images. Remote Sens. Environ., http://dx.doi.org/10.1016/0034-4257(92)90097-4.

Govender, M., Chetty, K., Bulcock, H., 2007. A review of hyperspectral remote sensing and its application in vegetation and water resource studies. Water SA, http://dx.doi.org/10.4314/wsa.v33i2.49049.

Hecker, C., Hook, S., van der Meijde, M., Bakker, W., van der Werff, H.M.A., Wilbrink, H., van Ruitenbeek, F., de Smeth, B., van der Meer, F.D., 2011. Thermal infrared spectrometer for Earth science remote sensing applications-instrument modifications and measurement procedures. Sensors 11, 10981–10999, http://dx.doi.org/10.3390/s111110981.

Horton, K.A., Johnson, J.R., Lucey, P.G., 1998. Infrared measurements of pristine and disturbed soils 2. Environ. Eff. Field Data Reduct. Remote Sens. Environ. 64, 47–52, http://dx.doi.org/10.1016/S0034-4257(97)00167-3.

Kahle, A.B., Alley, R.E., 1992. Separation of temperature and emittance in remotely sensed radiance measurements. Remote Sens. Environ. 42, 107–111, http://dx.doi.org/10.1016/0034-4257(92)90093-Y.

King, P.L., Ramsey, M.S., McMillan, P.F., Swayze, G.A., 2004. Laboratory Fourier transform infrared spectroscopy methods for geologic samples. In: King, P.L., Ramsey, M.S., McMillan, P.F., Swayze, G.A. (Eds.), Infrared Spectroscopy in Geochemistry, Exploration Geochemistry and Remote Sensing. Mineralogical Association of Canada, Quebec, QC, Canada.

Kirkland, L., Herr, K., Keim, E., Adams, P., Salisbury, J., Hackwell, J., Treiman, A., 2002. First use of an airborne thermal infrared hyperspectral scanner for compositional mapping. Remote Sens. Environ. 80, 447–459, http://dx.doi.org/10.1016/S0034-4257(01)00323-6.

Korb, A.R., Dybwad, P., Wadsworth, W., Salisbury, J.W., 1996. Portable Fourier transform infrared spectroradiometer for field measurements of radiance and emissivity. Appl. Opt. 35, 1679, http://dx.doi.org/10.1364/AO.35.001679.

Langley, S.K., Cheshire, H.M., Humes, K.S., 2001. A comparison of single date and multitemporal satellite image classifications in a semi-arid grassland. J. Arid Environ. 49, 401–411, http://dx.doi.org/10.1006/jare.2000.0771.

Nash, J., Sutcliffe, J., 1970. River flow forecasting through conceptual models part I—A discussion of principles. J. Hydrol. 10, 282–290, http://dx.doi.org/10.1016/0022-1694(70)90255-6.

Nicodemus, K.K., 2011. Letter to the editor: on the stability and ranking of predictors from random forest variable importance measures. Brief. Bioinf. 12, 369–373, http://dx.doi.org/10.1093/bib/bbr016.

OuYang, X., Wang, N., Wu, H., Li, Z., 2010. Errors analysis on temperature and emissivity determination from hyperspectral thermal infrared data. Opt. Express 18, 544, http://dx.doi.org/10.1364/OE.18.000544.

Ribeiro da Luz, B., Crowley, J.K., 2007. Spectral reflectance and emissivity features of broad leaf plants: prospects for remote sensing in the thermal infrared (8.0–14.0 μm). Remote Sens. Environ. 109, 393–405, http://dx.doi.org/10.1016/j.rse.2007.01.008.

Ribeiro da Luz, B., Crowley, J.K., 2010. Identification of plant species by using high spatial and spectral resolution thermal infrared (8.0–13.5 μm) imagery. Remote Sens. Environ. 114, 404–413, http://dx.doi.org/10.1016/j.rse.2009.09.019.

Ribeiro da Luz, B., 2006. Attenuated total reflectance spectroscopy of plant leaves: a tool for ecological and botanical studies. New Phytol. 172, 305–318, http://dx.doi.org/10.1111/j.1469-8137.2006.01823.x.

Riederer, M., Muller, C., 2006. Biology of the plant cuticle. Statewide Agric. Land Use Baseline 2015, http://dx.doi.org/10.1017/CBO9781107415324.004.

Salisbury, J.W., D'Aria, D.M., 1992. Infrared (8–14 μm) remote sensing of soil particle size. Remote Sens. Environ. 42, 157–165, http://dx.doi.org/10.1016/0034-4257(92)90099-6.

Salisbury, J.W., D'Aria, D.M., 1994. Emissivity of terrestrial materials in the 3–5 μm atmospheric window. Remote Sens. Environ. 47, 345–361, http://dx.doi.org/10.1016/0034-4257(94)90102-3.

Salisbury, J., 1986. Preliminary measurements of leaf spectral reflectance in the 8–14 μm region. Int. J. Remote Sens. 7, 1879–1886, http://dx.doi.org/10.1080/01431168608948981.

Schlerf, M., Rock, G., Lagueux, P., Ronellenfitsch, F., Gerhards, M., Hoffmann, L., Udelhoven, T., 2012. A hyperspectral thermal infrared imaging instrument for natural resources applications. Remote Sens. 4, 3995–4009, http://dx.doi.org/10.3390/rs4123995.

Silverstein, R.M., Webster, F.X., Kiemle, D.J., 2005. Spectrometric Identification of Organic Compounds., Spectrometric Identification of Organic Compounds Robert. John Wiley & Sons, inc, Hoboken, http://dx.doi.org/10.1021/ja00903a077.

Ullah, S., Groen, T.A., Schlerf, M., Skidmore, A.K., Nieuwenhuis, W., Vaiphasa, C., 2012a. Using a genetic algorithm as an optimal band selector in the mid and thermal infrared (2.5–14 μm) to discriminate vegetation species. Sens. (Basel) 12, 8755–8769, http://dx.doi.org/10.3390/s120708755.

Ullah, S., Schlerf, M., Skidmore, A.K., Hecker, C., 2012b. Identifying plant species using mid-wave infrared (2.5–6 μm) and thermal infrared (8–14 μm) emissivity spectra. Remote Sens. Environ. 118, 95–102, http://dx.doi.org/10.1016/j.rse.2011.11.008.

Ustin, S.L., Gamon, J.A., 2010. Remote sensing of plant functional types. New Phytol. 186, 795–816, http://dx.doi.org/10.1111/j.1469-8137.2010.03284.x.

Vaughan, R.G., Calvin, W.M., Taranik, J.V., 2003. SEBASS hyperspectral thermal infrared data: surface emissivity measurement and mineral mapping. Remote Sens. Environ. 85, 48–63, http://dx.doi.org/10.1016/S0034-4257(02)00186-4.

Wang, X., Ouyang, X., Tang, B., Li, Z., Zhang, R., Ensps, L., Brant, B.S., 2008. A new method for temperature/eEmissivity separation from hyperspectral thermal infrared data. Sci. York, 286–289.

White, M.A., Hoffman, F., Hargrove, W.W., 2005. A global framework for monitoring phenological responses to climate change 32, 2–5. doi:10.1029/2004GL021961.

Wilson, E.B., Decius, J.C., Cross, P.C., Sundheim, B.R., 1955. Molecular vibrations: the theory of infrared and raman vibrational spectra. J. Electrochem. Soc. 102, 235C, http://dx.doi.org/10.1149/1.2430134.